Common-Path Fourier-Domain Optical Coherence Tomography using Surface Tracking Algorithm

C. G. Song[1], K. S. Kim[1], M. H. Kim[1], S. H. Ryu[1], J. H. Seo[2]
[1] Div. of Electronics Eng., Chonbuk Natl. Univ., Korea
[2] Dept. of Rehabilitation Med., Chonbuk Natl. Univ. Hospital, Korea

Abstract - *Conventional optical coherence tomography (OCT) systems generally have a limited imaging range within a depth of only 1-2 mm and suffers from unwanted noise such as speckle, ghost or mirror noise. To overcome these limitations, we developed a motorized-stage-based OCT system with an extended imaging range, using a common-path Fourier-domain optical coherence tomography (CP-FD-OCT) configuration. Using this OCT systems, OCT image was obtained from an onion, and their subsurface structure were observed. The result showed that the OCT images obtained using our motorized-stage-based system had a significantly extended imaging range due to its real-time accurate depth tracking. Consequently, the devised CP-FD-OCT systems and algorithms have good potential for the further development of endoscopic OCT for microsurgery.*

Keywords: OCT, Common-path OCT, FD-OCT, Tracking algorithm

1   Introduction

Optical coherence tomography (OCT), which is one of the various optical imaging modalities, is a novel imaging technology that provides high- resolution, subsurface depth profiling, and cross-sectional imaging in vivo with relatively simple optical arrangements and an inexpensive light source in a non-invasive manner. The concept of OCT and its application were first introduced by Fujimoto et al. in 1991 [1]. OCT imaging is somewhat analogous to the B-scan imaging technique based on ultrasound, except that it uses light instead of sound.

This technique typically makes use of a Michelson interferometer and allows a depth-profile to be obtained by measuring the optical pathlength or phase difference between the reflected or backscattered light beam and a reference one, when near infra-red light (wavelength: 600-1,300 nm) is illuminated onto the sample. First, the light generated from the light source is divided into two arms, viz. the sample arm used for exploring the sample and the reference arm which is usually obtained using a mirror, via a beam splitter or optical coupler. Next, the combination of the reflected or backscattered light from the sample arm and reference light gives rise to an interference pattern. The more light that is reflected back from the reflective layer within the sample, the greater the intensity of the interference fringe. This reflectivity profile (A-scan) contains information about the spatial dimensions and location of the structures within the sample of interest and, thus, OCT images can be obtained by measuring the optical delay according to the depth within the sample, i.e. different reflective loci at different depths in the sample. Finally, a cross-sectional image (B-scan) may be achieved by laterally combining a series of these axial depth profiles.

The OCT technique has several benefits for the non-invasive, high-resolution and fast-acquisition tomography of the internal microstructure in biological systems and materials. First of all, it can provide much higher-resolution images (2-10 μm) than conventional imaging techniques, such as ultrasound (over 500 μm), MRI and CT (over 100 μm), although its depth information is limited to a range of approximately 2-3 mm in turbid tissue [2]. Also, OCT has a faster scanning speed for acquisition and relatively wider dynamic range [3]. OCT can image with an acquisition rate of up to 20 frames per second, which should allow this technology to image surgical procedures in near real time. Moreover, the entire system is simple and portable and, thus, has the potential to enable OCT catheters to be incorporated into endoscopic instruments or bedside devices. Finally, since OCT is based on optics, it can be combined with other spectroscopic techniques to assess the optical and biochemical aspects of the tissue being imaged.

Common-path OCT (CP-OCT) was proposed by Vakhtin et al. in 2003 [4]. In the CP-OCT configuration, the beam paths, which the sample signals backscattered from the sample and reference signals reflected from the reference plane follow, are commonly shared, thereby

eliminating the need for the reference arm in the interferometer. This modality can minimize the effect caused by the mismatch of the polarization and dispersion states between the optical elements in the interferometer and the sensitivity to vibration, and enhance the scanning speed, simplicity and system robustness. Consequently, this configuration has the potential to be used as a microsurgical tool. Some researchers have reported the feasibility of an endoscopic CP-OCT implementation based on the common-path modality [5-7].

However, unfortunately, most OCT systems generally suffer from a limited imaging depth range of only 1-3 mm, depending on the tissue type and, thus, this limitation restricts their clinical applications when the sample's topological variance is larger than the imaging depth range [8]. To overcome these limitations, some techniques such as the adaptive ranging technique based on depth tracking have been proposed in previous papers [9-10]. In these methods, the coherence gate offset and range on the reference arm are adaptively adjusted by means of an active tracker consisting of various optical lenses and a galvanometer. Also, alternative techniques using an auxiliary spectral domain partial coherence interferometer [11], tunable endoscopic MEMS probe consisting of a pneumatically-actuated micro-lens and a GRIN lens [12], or dual reference arms and a high-speed fiber optic switch [13] were attempted. However, these techniques require the supplementary alignment of the various optical lenses or components and synchronization control and, thus, the composition and control procedure of the OCT system might become more onerous and complicated. Also, they compensate for the topological variance and motion by adjusting the optical pathlength on the reference arm and, therefore, this strategy might be inappropriate for the CP-FD-OCT system constructed in this study, since CP-OCT uses the common beam path of the sample and reference signal instead of using the reference mirror used in the conventional OCT composition. Recently, Zhang et al. [14] reported a CP-FD-OCT system providing a surface topology and motion compensation technique in the axial direction by means of a 1-D erosion-based edge-searching algorithm, which makes use of the relatively simple signal processing of the A-scan data instead of the alignment of complex optical components.

To assess the feasibility of the system described in this paper, an active compensation algorithm of the topological variance by means of a sample surface detection algorithm using a Savitzky-Golay smoothing filter and feedback control for adjusting continuously the position of the motorized stage was developed in the present study. This algorithm makes it possible to image a deeper range along the z-axis by keeping the distance between the end of the probe and the sample's surface constant, as compared to the conventional scanning strategies.

2 FD-CP-OCT system

2.1 Hardware Configuration

To obtain high-resolution OCT images with an extended range of imaging depths, a motorized-stage-based OCT system was developed. It consists of a high-resolution spectrometer, actively controllable motorized-stage, actuators and control modules, as well as basic compositions such as a light source, 50/50 coupler, and single mode fiber-optic probe. Figure 1 shows the block diagram of the developed CP-FD-OCT system. A superluminescent diode (SLD) (SLD-351, Superlum Diode Ltd., Ireland) with a central wavelength of 860 nm and spectral full-width at half maximum (FWHM) of ~60 nm was used as the light source. A 50/50 coupler (FC850-40-50-APC, Thorlabs Inc., U.S.) was used as the beam splitter, and only one branch on the right side was used as the common path for the signal and reference. The single mode fiber-optic probe constructed in this study was fixed on a standing vise, with A-scan (z-axis) and B-scan (x-axis). The
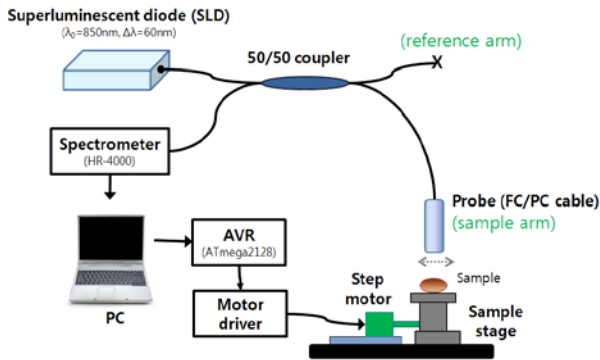

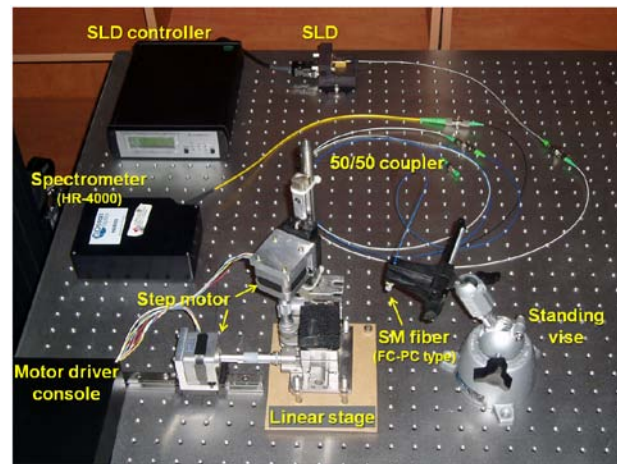Fig 1. Block diagram of the developed CP-FD-OCT system.

Fig 2. Photograph of the developed CP-FD-OCT system.

two axes of the x and z directions were driven by a motorized stage (M-561D-XYZ, Newport Corp., U.S.) with two separate step motors (SE-SM243, N.T.C., Korea) installed on its lateral side. The reference signal came from the Fresnel reflection at the fiber probe end and the sample signal and the reference were received by a high-speed spectrometer (HR-4000, Ocean Optics, U.S.) with a charge-coupled device detector array with 3648 pixels covering a range of 700-900 nm. This system make it possible to extend the imaging range, since the position of the probe can be adjusted actively and simultaneously according to the sample's topological variance, whereas the time needed for image acquisition is relatively longer. Figure 2 shows the photograph of the developed system.

2.2   Software configuration

To control the actuators and perform image processing in our motorized-stage-based CP-FD-OCT system, OCT acquisition software was developed using the LabVIEW language (ver. 8.6, National Instruments, U.S.) based on a graphic user interface (GUI) with buttons and graphs.

Figure 3 shows the developed software. The 'New Reference' button is used for measuring the reference signal in the CP-OCT configuration. The 'B-scan' button is used for obtaining the B-scan OCT image, while 'Stop' is used for holding the B-scanning. The 'Reset' button is used for initializing variables such as the rotation speed and period of the actuator per step, B-scanning range, and set-up distance between the probe and sample's surface and so on. Also, the 'Save' and 'Load' buttons are used for storing the measured OCT image on the host PC and loading the OCT image file from the PC, respectively. 'Exit' is used to terminate the software.

The lateral resolution, which means the lateral displacement per A-scan data, and total B-scan range are given by inputting the information into the combo ('Set step degree') and control boxes ('Distance') on the top left of the
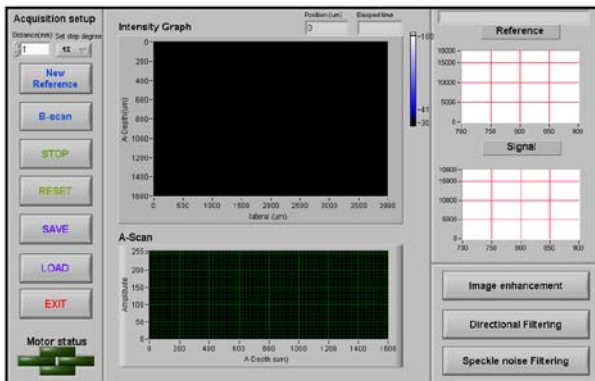
screen, respectively. Also, the position of the stage can be manually adjusted by repeatedly entering the keyboard keys, '△' (upward), '▽' (downward)', '▷' (forward), or '◁' (backward), and then the moving direction of the stage is instantly indicated by the corresponding LED at the bottom left of the screen.

The instant spectral distribution and A-scan data measured during B-scanning are simultaneously displayed in the corresponding graphs of 'Signal' in the middle right and 'A-scan' in the bottom center, respectively. At the end of B-scanning, the final 2D OCT image is displayed on the 'Intensity Graph' in the top center.

2.3   Active surface tracking algorithm

Figure 4 shows a flow chart of the active topological variance compensation algorithm during B-mode scanning in CP-FD-OCT, while the distance from the sample's surface exceeds the OCT imaging depth range or when the probe is too close to the sample.

In 'Step-1', the A-scan data, a(z) is obtained from the probe (N is the total length of a(z), as shown in Figure 5(a).

In 'Step-2', the distance (Dist) between the end of the probe and the sample's surface is determined, as follows; i) a(z) is smoothed by a 3rd-order Savitzky-Golay filter (its

Fig 3. Photograph of the developed OCT acquisition software.
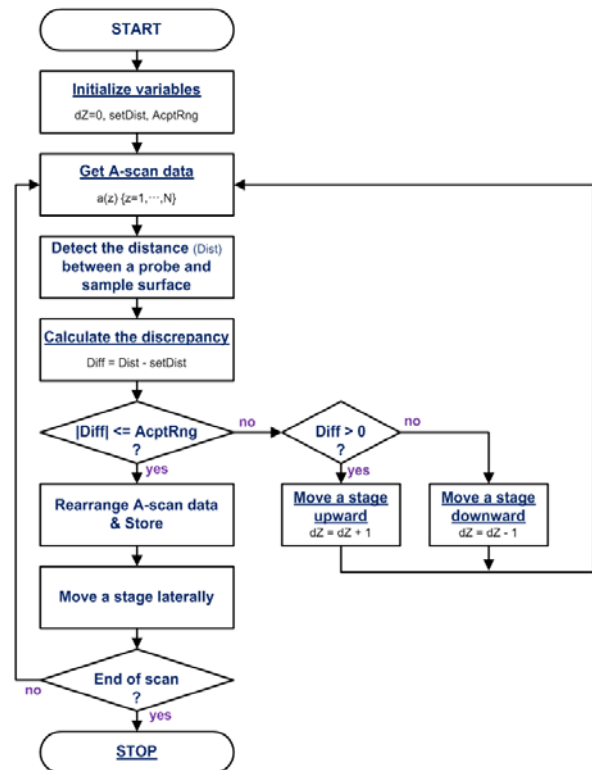

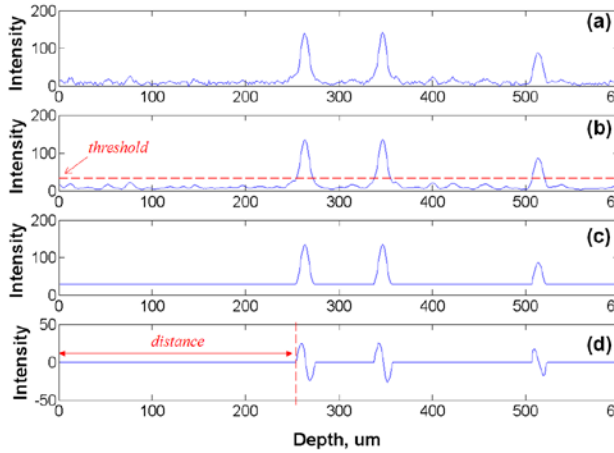Fig 4. Flow chart for active surface tracking algorithm.

Fig 5. Active surface tracking algorithm. (a) Raw A-scan data, (b) A-scan data after Savitzky-Golay smoothing filter, (c) Thresholding of A-scan, and (d) First increment point detection for edge location.

window length is 9), as shown in Figure 5(b). The main advantage of the Savitzky-Golay filter used in this algorithm is that it can preserve the unique features of the distribution, such as the relative maxima, minima and width, which are usually flattened by other adjacent averaging techniques, such as a moving average or low-pass filter, as well as effectively reducing the unnecessary speckle noise [15], as shown in Figure 6. This attribute is quite useful for the more accurate detection of the edges from the A-scan data and, thus, over- or under-estimation of the distance can be effectively diminished compared to the other smoothing methods. ii) the smoothed A-scan data, asm(z), is processed using a certain threshold level (thre) to avoid the noise effect, as follows (Figure 5(c));
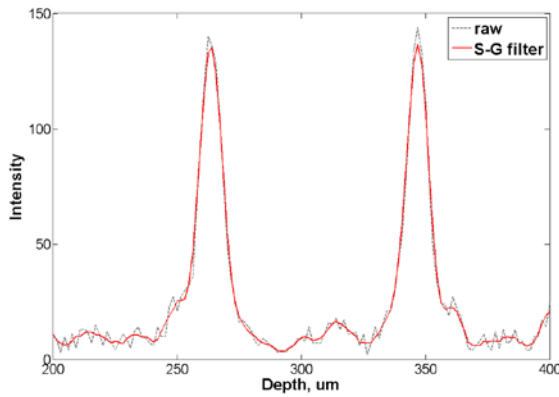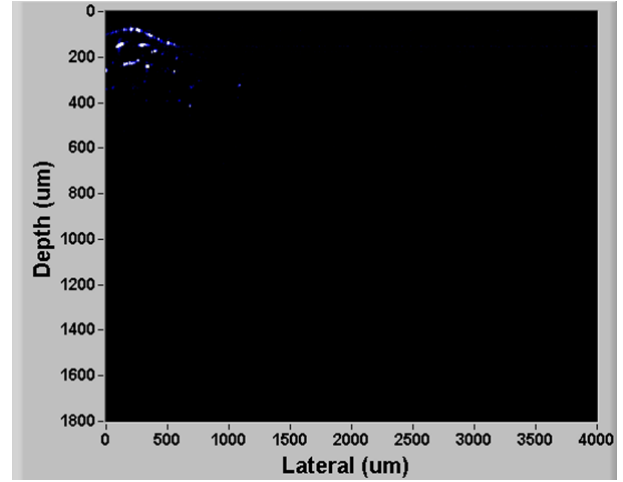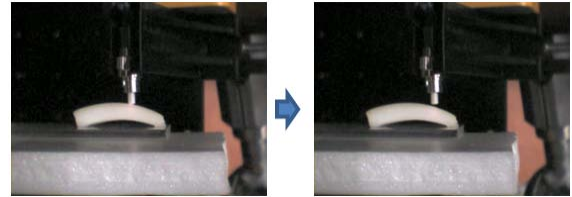

Fig 6. Comparison the raw A-scan data (dotted line) and smoothed one after Savitzky-Golay filter (solid line).

(a) OCT image

(b) Probe position at the start (*left*) and end times (*right*) of the lateral scan

Fig 7. Image of an onion sample obtained by the conventional static stage on the z-axis with limited imaging depth.

$$a_{thre} = \begin{cases} a_{sm}(z), & a_{sm}(z) > thre \\ thre, & others \end{cases} \qquad (1)$$

iii) Dist is given by the first increment point of the differential of the post-thresholding data, as shown in Figure 5(d).

In 'Step-3', the discrepancy (Diff) between the preset (setDist) and measured (Dist) distances is calculated, as follows;

$$Diff = Dist - setDist \qquad (2)$$

In 'Step-4', by using the Diff value obtained in 'Step-3', the control system sends the feedback control signal to the motorized stage. If the absolute value of Diff is outside of the preset acceptable range (AcptRng), the stage is moved either upward for a positive value of Diff or downward for a negative value of Diff. Subsequently, 'Step-1' is performed again until Diff is within AcptRng. On the other hand, if it is within AcptRng, the measured a(z) is rearranged and stored in memory. During recording, the values of a(z) are repeatedly obtained while maintaining a constant distance

between the end of the probe and the sample's surface and, thus, this a(z) can be rearranged by considering the practically moved height of the stage. The variable, dZ, is used for counting the relative displacement at the current position compared to that at the start of the B-scan (dZ=0) on the z-axis. For example, a positive value of dZ indicates that the probe has moved closer to the sample, so it implies that the practical depth of the OCT image might be relatively larger than that of the measured a(z), whereas a negative dZ means that the practical depth of the OCT image is relatively smaller than that of the measured a(z).

In 'Step-5', the stage is moved laterally for one step, and 'Step-1' is performed again until the moved position of the stage is the end of the scan on the x-axis.
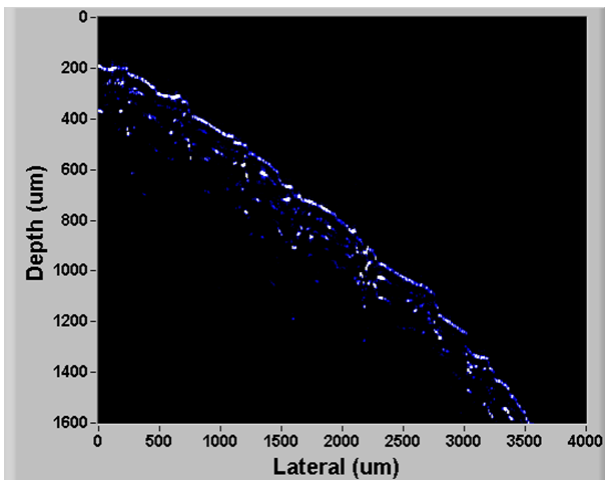
(a) OCT image
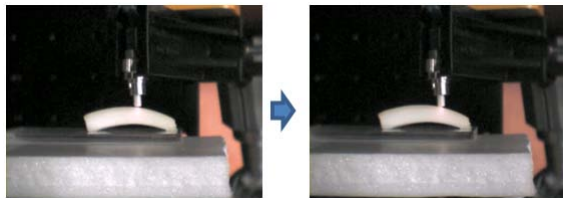
(b) the probe position at the start (*left*) and end times (*right*) of the lateral scan

Fig 8. Image of an onion sample by the active topological variance compensation algorithm with extended imaging depth. (a) OCT image, (b) the probe position at the start (*left*) and end times (*right*) of the lateral scan.

3 Results and Discussions

The performance of the active topology compensation algorithm was tested under static conditions using an onion sample with several layers of highly curved surfaces. At first, a B-scan 2-D OCT image was obtained by the conventional fixed-stage method, as shown in Figure7(a).

The 860 nm CP-FD-OCT provided effective imaging in the range below 500 nm and the structure of some of the layers was very clear within this range. However, the OCT image fades away as the probe is moved further away from the sample's surface, due to the limited depth range, as shown in Figure 7 (b).

Figure 8 (a) shows an improved OCT image obtained using the active topological variance compensation algorithm. By using our algorithm, the probe could actively track the sample surface variance, as shown in Figure 8 (b) and, consequently, the effective imaging depth was extended to the probe's free-moving range. Also, the sub-layers of the sample could be monitored more clearly, even if the distance between the probe and sample's surface was outside of the limited imaging range.

4 CONCLUSION

We developed CP-FD-OCT systems with an active surface tracking algorithm to extend the image range of OCT scanning. Consequently, the OCT images obtained using the motorized-stage-based system showed a significantly extended imaging range through real-time accurate depth tracking. These results demonstrate that our OCT system and algorithms have good potential to resolve several of the limitations of conventional OCT systems.

5 REFERENCES

[1]   D. Huang, E. A. Swanson, C. P. Lin, J. S. Schuman, W. G. Stinson, W. Chang, M. R. Hee, T. Flotte, K. Gregory, C. A. Puliafito, J. G. Fujimoto, "Optical coherence tomography," Science, vol. 254, no. 5035, pp. 1178-1181, 1991.

[2]   S. A. Boppart, B. E. Bouma, C. Pitris, J. F. Southern, M. E. Brezinski, J. G. Fujimoto, "In vivo cellular optical coherence tomography imaging," Nat. Med., vol. 4, no. 7, pp. 861-865, 1998.

[3]   G. J. Tearney, M. E. Brezinski, B. E. Bouma, S. A. Boppart, C. Pitris, J. F. Southern, J. G. Fujimoto, "In vivo endoscopic optical biopsy with optical coherence tomography," Science, vol. 276, no. 5321, pp. 2037-2039, 1997.

[4]   B. Vakhtin, D. J. Kane, W. R. Wood, K. A. Peterson, "Common-path interferometer for frequency-domain optical coherence tomography," Appl. Optics, vol. 42, no. 34, pp. 6953-6958, 2003.

[5]   R. Tumlinson, J. K. Barton, B. Povazay, H. Sattman, A. Unterhuber, R. A. Leitgeb, W. Drexler, "Endoscope-tip interferometer for ultrahigh resolution frequency domain

optical coherence tomography in mouse colon," Opt. Express, vol. 14, no. 5, pp. 1878-1887, 2006.

[6] U. Sharma, J. U. Kang, "Common-path optical coherence tomography with side-viewing bare fiber probe for endoscopic optical coherence tomography," Rev. Sci. Instrum., vol. 78, no. 11, pp. 113102, 2007.

[7] K. M. Tan, M. Mazilu, T. H. Chow, W. M. Lee, K. Taguchi, B. K. Ng, W. Sibbett, C. S. Herrington, C.T. A. Brown, K. Dholakia, "In-fiber common-path optical coherence tomography using a conical-tip fiber," Opt. Express, vol. 17, no. 4, pp. 2375-2384, 2009.

[8] Low, G. Tearney, B. Bouma, I. Jang, "Technology insight: Optical coherence tomography - Current status and future development," Nat. Clin. Pract. Card., vol. 3, no. 3, pp. 154-162, 2006.

[9] N. Iftimia, B. Bouma, J. F. de Boer, B. Park, B. Cense, G. Tearney, "Adaptive ranging for optical coherence tomography," Opt. Express, vol. 12, no. 17, pp. 4025-4034, 2004.

[10] G. Maguluri, M. Mujat, B. Park, K. Kim, W. Sun, N. Iftimia, R. Ferguson, D. Hammer, T. Chen, J. Boer, "Three dimensional tracking for volumetric spectral-domain optical coherence tomography," Opt. Express, vol. 15, no. 25, pp. 16808-16817, 2007.

[11] M. Pircher, B. Baumann, E. Götzinger, H. Sattmann, C. K. Hitzenberger, "Simultaneous SLO/OCT imaging of the human retina with axial eye motion correction," Opt. Express, vol. 15, no. 25, pp. 16922-16932, 2007.

[12] K. Aljasem, A. Werber, H. Zappe, "Tunable endoscopic MEMS-probe for optical coherence tomography," Proc. 2007 IEEE/LEOS Int. Conf. Optical MEMS and Nanophotonics, pp. 8-9, Hualien, Taiwan, 2007.

[13] [13] H. Wang, Y. Pan, A. M. Rollins, "Extending the effective imaging range of Fourier-domain optical coherence tomography using a fiber optic switch," Opt. Lett., vol. 33, no. 22, pp. 2632-2634, 2008.

[14] K. Zhang, W. Wang, J. Han, J. U. Kang, "A surface topology and motion compensation system for microsurgery guidance and intervention based on common-path optical coherence tomography," IEEE T. Biomed. Eng., vol. 56, no. 9, pp. 2318-2321, 2009.

[15] J. Luo, K. Ying, J. Bai, "Savitzky-Golay smoothing and differentiation filter for even number data," Signal Process., vol. 85, no. 7, pp. 1429-1434, 2005.